frontiers | Frontiers in Materials

TYPE Original Research
PUBLISHED 19 December 2022
DOI 10.3389/fmats.2022.1094696

OPEN ACCESS

EDITED BY
Zhigang Zhang,
Chongqing University, China

REVIEWED BY
Tengfei Xu,
Southwest Jiaotong University, China
Haijun Wu,
Chongqing Jiaotong University, China

*CORRESPONDENCE
Yin Shen,
shenyin@tongji.edu.cn

SPECIALTY SECTION
This article was submitted to Structural Materials, a section of the journal Frontiers in Materials

RECEIVED 10 November 2022
ACCEPTED 06 December 2022
PUBLISHED 19 December 2022

CITATION
Huang G, Wu B, Shen Y, Wang L and Li G (2022), Comparative experiment of steel bar corrosion at concrete construction joints.
Front. Mater. 9:1094696.
doi: 10.3389/fmats.2022.1094696

Comparative experiment of steel bar corrosion at concrete construction joints

Guohua Huang[1], Binzhong Wu[1], Yin Shen[2]*, Li Wang[1] and Guoping Li[2]

[1]Powerchina Roadbridge Group Co., LTD, Beijing, China, [2]College of Civil Engineering, Tongji University, Shanghai, China

Introduction: Construction joint is common and even inevitable in most of the reinforcement concrete structures. This study was to assess the effect of construction joints on chloride-induced corrosion of reinforcing steel in concrete.

Methods: Test parameters included two environmental conditions (salt solution immersion condition and cyclic wet-dry condition), two forms of construction joint (direct wet joint and roughened wet joint) and four types of steel bar (mild steel bar, ferritic stainless-steel bar, austenitic-ferritic stainless-steel bar and epoxy-coated steel bar). The corrosion test of 90 specimens was carried out by electrochemical accelerated corrosion method. The weight loss of each steel bar and steel bar section in specimens was measured. An influence coefficient (k_j) of construction joint on local weigh loss of steel bars was defined.

Results: Except for epoxy-coated steel bars, the most severe corrosion of experimental steel bars in concrete specimens all occurred at the joints, while the corrosion in non-joint sections of steel bars was relatively uniform and less. The weight loss rate of specimens has the range of 1.18% to 15.73% with an average value of 6.22%. The average k_j of mild steel bars, S11203 stainless steel bars, and S23043 stainless steel bars are 1.38, 1.92, and 1.97, respectively. The average k_j of specimens in immersion condition and cyclic wet-dry condition are 1.44 and 2.07. The corrosion of epoxy-coated steel bars mainly occurred at the damage locations of epoxy coating, not mainly at the joints.

Conclusion: Chloride-induced corrosion of steel bars at construction joints was always more severe than at non-joints, especially in cyclic wet-dry environments, even for stainless-steel bar, but epoxy-coated steel bars were excluded.

KEYWORDS

construction joint, steel bar corrosion, electrochemical acceleration corrosion, immersion, wet–dry cycle

1 Introduction

Reinforced concrete structures are widely used in coastal engineering. Many studies have shown that the durability failure of reinforced concrete structures in the marine environment is mainly due to the corrosion of reinforcement in concrete (Goyal et al., 2018; Choe et al., 2020). In the literature, many researches have been performed on reinforcement corrosion in continuously casted concrete members (Guoping et al., 2011; Andrade 2019). However, due to the concrete construction methods and capacity of mixing plan and manpower, it is very common for concrete to be poured in segments or batches in reinforced concrete structures (Sung-Won and Seung-Jun 2016). Construction joints are concrete-to-concrete interfaces formed by placing fresh or hardened concrete parts against a hardened concrete substrate.

From the literature, construction joint is also a kind of cold joint (Yoon et al., 2020). Kara (2021) conducted strength and durability tests on concrete with cold joints and found that after dry-wet cycles, the weight loss of concrete with cold joints was greater than that of the monolithic concrete sample, and the tensile strength loss rate was 42.07%. Zega et al. (2021) experimented and found that the cold joint in normal concrete had a decrease in flexural and compressive strength, so did with the concrete with superplasticizer. Vanlalruata and Marthong (2021) conducted flexural strength tests of 40 beams and showed that the loss in flexural strength due to the present of cold joint in a reinforced concrete beam ranges from 2% to 20% for different mix and age of the joints. Those indicated that the concrete with cold joint is more prone to cracking under working conditions because of the loss of tensile strength, which accelerates the degradation of concrete (Yang et al., 2018).

Moreover, Li et al. (2017) conducted a series of accelerated carbonation tests and proved that the carbonation depth of concrete at a construction joint was higher than that of monolithic concrete even in the absence of tensile stress. Several salt solution immersion tests showed that the chloride penetration at a construction joint was faster. Mun and Kwon (2016) presented an evaluation of cold joint and loading conditions on chloride diffusion behavior, and the study showed that chloride diffusion coefficient under 30% level of compressive stress significantly increases by 1.7 times compared with normal condition. Li et al. (2016) conducted a salt solution immersion test on six specimens with direct wet joints, roughened wet joints and epoxied joints and conclude that monolithic concrete had optimal resistance to chloride ions, better than the direct wet joints and roughened wet joints. Shen et al. (2019) conducted a freeze–thaw cycle test in the laboratory and found that construction joints increased the mass loss of specimens. Many studies have pointed out that construction joint may become the weakness of concrete durability. Therefore, the steel bars at the construction joints are relatively easier to contact with chloride ions, water vapor, oxygen and other substances that accelerate the corrosion of steel bars (Koh et al., 2019). Once the harmful substances reach the critical concentration, the steel bars will begin to rust at the construction joints, reducing the effective section areas of the steel bars and endangering the durability and safety of the structure.

For the study of steel corrosion, most of them use electrochemical technology. In the 1950s, electrochemical techniques were applied to study the corrosion of steel in cement-based materials (Stern and Geaby 1957). In the study of durability of reinforced concrete structures, electrochemical technology is basically used to accelerate the corrosion of steel bars in concrete. Although it must be noted that there are obvious differences between electrochemical accelerated corrosion and natural corrosion in terms of electrochemical mechanism, corrosion products and corrosion morphology (Song et al., 2008), electrochemical accelerated corrosion can qualitatively characterize the degradation of structural performance. With the development of durability research, electrochemical technology has been applied to the study of mechanical properties of corroded steel bars, bond-slip performance of corroded reinforced concrete (Zhou et al., 2015; Zhou et al., 2017), structural performance degradation of reinforced concrete beams (Ou and Nguyen 2016) and piers (Yuan et al., 2018; Zhou et al., 2020). At present, many specifications are based on the data of electric accelerated corrosion method for the deformation calculation, mechanical performance evaluation and life prediction theory of corroded reinforced concrete members.

Many tests have pointed out that the construction joints have a negative effect on the durability of concrete, and the conclusions are based on indicators such as carbonation coefficient and chloride diffusivity. However, the corrosion propagation test of steel bars at the joints that can accurately represent the performance degradation of concrete structures has not been reported. Therefore, this paper explored the corrosion morphology of steel bars at joints, compared the difference of steel bar rust amount at joints and non-joints, and investigated the corrosion characteristics of different steel bars at joints. The comparative test in this paper was to provide basic test data and reference for further research and helped engineers to further understand the impact of construction in harsh marine environment on the long-term corrosion resistance of important infrastructure such as bridges.

The present study mainly focuses on the comparison of steel corrosion test phenomena at construction joints and the analysis and interpretation of measured data under different steel bar types, joint types and different environments. The material transportation at construction joints will be examined in a future study by means of meso-scale numerical simulation.

2 Materials and methods

2.1 Materials

The concrete material and mix proportions are listed in Table 1. Crushed stone with maximum aggregate size distributed from 5 to 25 mm was used as the coarse aggregate. River sand with a fineness

TABLE 1 Concrete material and mix proportions.

Concrete strength[a] (MPa)	Water/cement ratio	Cement (kg)	Fine aggregate (kg)	Coarse aggregate (kg)	Water (kg)	Water reducer (%)
49.99	0.36	482	598	1147	173	0.8

[a]Concrete strength is the average cubic compressive strength of three 150 mm test cubes.

TABLE 2 Chemical composition of rebars.

Steel type	Chemical composition (%)									
	C	Si	Mn	P	S	Ni	Cr	Mo	Cu	N
MS/EP	0.25	0.8	1.6	0.045	0.045	—	—	—	—	—
S11203	0.03	1.0	1.0	0.04	0.03	0.6	11.0	—	—	—
S23043	0.03	1.0	2.5	0.035	0.03	3.00	21.5	0.05	0.05	0.05

Note: MS, mild steel rebar; EP, epoxy-coated steel rebar; S11203, ferritic stainless steel rebar (named S11203 in GB/T 20878-2007, China); S23043, austenitic-ferritic (duplex) stainless steel rebar (named S23043 in GB/T 20878-2007, China).

TABLE 3 Details of parameters and quantities.

Condition	Joint type	Steel bar type	Id	Quantity
Immersion	Roughened wet joint	Mild steel	IC-RJ-MS	6
		Epoxy-coated steel	IC-RJ-EP	5
		Stainless steel S11203	IC-RJ-S11203	5
		Stainless steel S23043	IC-RJ-S23043	5
	Direct wet joint	Mild steel	IC-DJ-MS	6
		Epoxy-coated steel	IC-DJ-EP	5
		Stainless steel S11203	IC-DJ-S11203	5
		Stainless steel S23043	IC-DJ-S23043	5
Wet–dry cycle	Roughened wet joint	Mild steel	WD-RJ-MS	6
		Epoxy-coated steel	WD-RJ-EP	6
		Stainless steel S11203	WD-RJ-S11203	6
		Stainless steel S23043	WD-RJ-S23043	6
	Direct wet joint	Mild steel	WD-DJ-MS	6
		Epoxy-coated steel	WD-DJ-EP	6
		Stainless steel S11203	WD-DJ-S11203	6
		Stainless steel S23043	WD-DJ-S23043	6

Note: IC, immersion condition; WD, wet–dry cycle condition; RJ, roughened wet joint; DJ, direct wet joint.

modulus of 2.71 was chosen as the fine aggregate in the mixes. The water/cement ratio for the mixtures was 0.36.

All test rebars were ribbed with a diameter of 16 mm and yield design strength of 400 MPa. The chemical composition of rebars are listed in Table 2.

2.2 Test parameters

A total of 16 categories were considered, including 90 specimens. A construction joint was made in the middle of each specimen, and the specimens were long enough, so that both

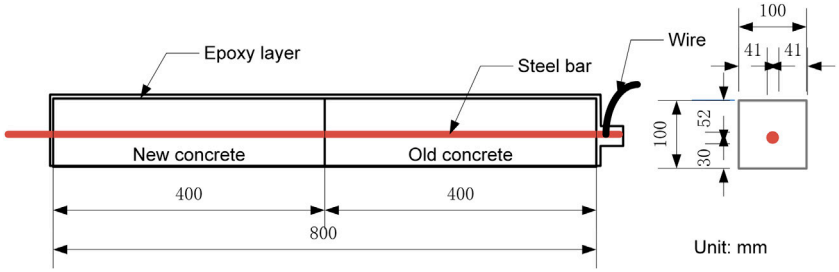

FIGURE 1
Specimen dimensions.

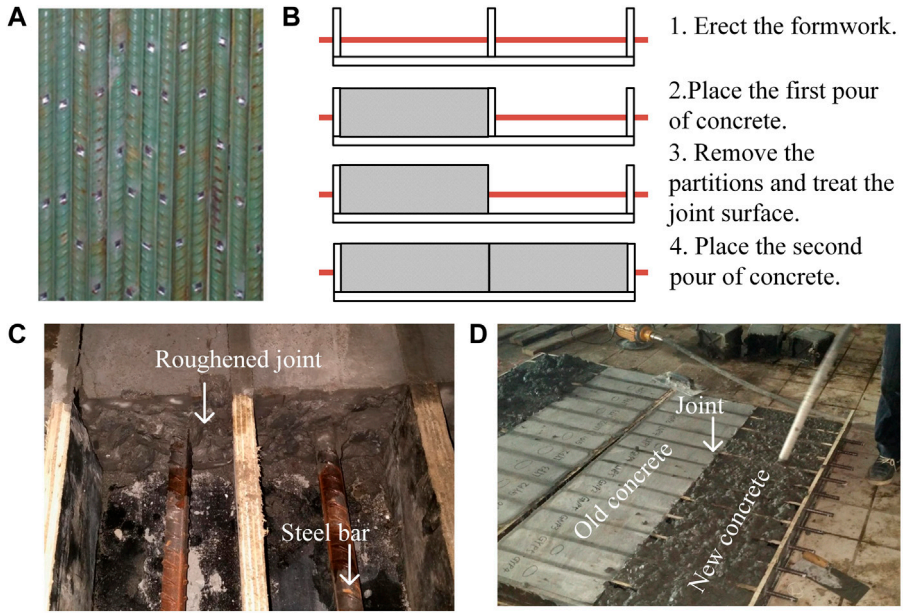

FIGURE 2
Specimen preparation. **(A)** Epoxy-coated rebars. **(B)** Fabrication process. **(C)** Roughened interface at joint. **(D)** Specimen casting.

side parts of specimens that didn't contain joints could be as control parts, and the test conditions were exactly the same, so this experiment didn't design separate control specimens. The experimental parameters are described as follows:

1) Two marine environmental conditions (James et al., 2019) were selected, namely a chlorine salt solution immersion condition and a cyclic wet–dry condition. The former was used to simulate a seawater immersion environment, and the latter was used to simulate the tidal environment.
2) Two forms of construction joint were studied, the direct wet joint and roughened wet joint (Júlio et al., 2004). Direct wet joint refers to a joint formed by pouring fresh concrete directly without special treatment on the substrate surface, while roughened wet joint refers to a joint with a substrate surface roughened by jack hammers.
3) Four types of rebar were tested: mild steel bar, ferritic stainless-steel bar (named S11203 in GB/T 20878-2007, China), austenitic-ferritic (duplex) stainless-steel bar (named S23043 in GB/T 20878-2007, China), and epoxy-coated rebar. These are the main types of rebar commonly used in concrete structures in marine and coastal harsh environments (Lollini et al., 2019).

The experimental categories and specimen quantities are listed in Table 3.

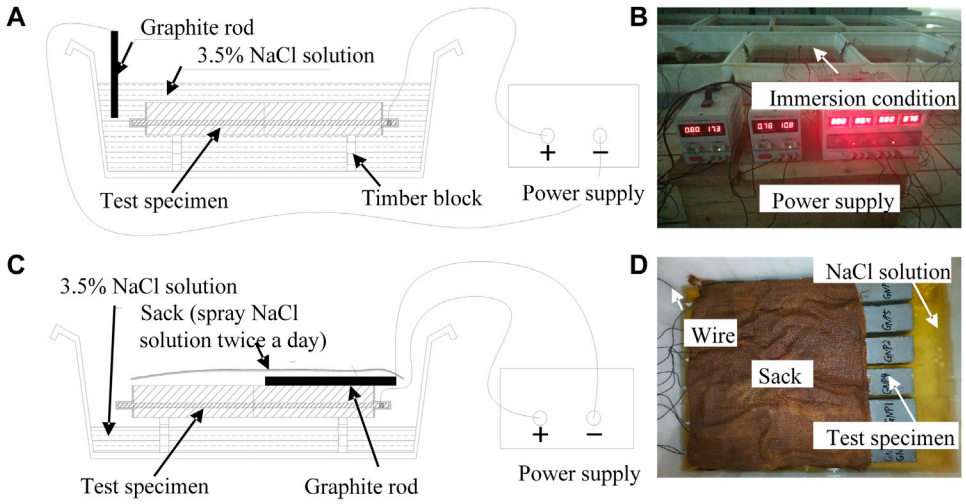

FIGURE 3
Electrochemically accelerated corrosion. **(A,B)** Immersion condition. **(C,D)** Wet–dry cycle condition.

2.3 Specimen fabrication

The design of specimens referred to the Standard for Testing the Long-Term Performance and Durability of Ordinary Concrete (GB/T 50082-2009, China). Thus, the dimensions 100 × 100 × 800 mm were selected for concrete prism specimens. A construction joint was located in the middle of each specimen as shown in Figure 1. The concrete cover thickness of the steel bar at the bottom was designed as 30 mm. The bottom surface of the specimen was set as the exposed face to experimental conditions, and the side and top surface were sealed with epoxy resin to avoid the intrusion of chloride ions.

The length of each rebar was 900 mm. First, all mild steel and stainless-steel bars were polished to remove the rust spots. For epoxy-coated rebars (Figure 2A), man-made scratches were added to the epoxy coating to simulate irregular damage in the transportation of epoxy rebars and concrete construction. The epoxy coating at scratches was completely damaged and the substrate was exposed. The size of a scratch was about equal to the rib spacing of rebar and the scratches was evenly distributed. The ratio of coating damage was about 5%. Then, all rebars were labeled and the length and weight were accurately measured.

Each specimen was molded in two parts and the fabrication process is shown in Figure 2B. The part of old concrete was first casted. After 3 days, all partitions at joints were removed. In 2 days, the joint interface on old concrete of each specimen with roughened joint was artificially scabbled as shown in Figure 2C, and kept in a saturated surface dry state according to current construction practice in China. Then the part of new concrete was placed as shown in Figure 2D. After three more days, all formworks were removed, and all specimens were placed in a standard maintenance room with a temperature of 20°C ± 2°C and a relative humidity of 95% for 28 days.

2.4 Test method

The comparative experiments were carried out by the electrochemical acceleration corrosion method. Direct current in a parallel manner was used to accelerate corrosion, as shown in Figure 3.

For Group IC in the immersion condition, all specimens directly and completely immersed in chlorine salt solution (Figures 3A, B). Given that the salinity of seawater is of 3.5% NaCl, a 3.5 wt% NaCl solution was used for corrosion experiments. As the water in the basin evaporated, the solution level in the basin was checked every 3 days and the water was supplemented in time. The steel bar was connected with the positive electrode of the steady voltage DC power supply as the anode of the electrochemical reaction; the graphite rod was directly placed in the solution as a cathode.

For Group WD in the dry-wet cycle condition, all specimens were supported by bolsters above the chloride solution (Figures 3C, D), and the same solution was sprayed periodically onto the specimens twice a day. Graphite rod as cathode, directly flat on the top of the specimen. In order to prevent the solution from evaporating too quickly and length of exposure to the humid environment being too short after spraying, a layer of gauze was spread on specimens, and a thick cotton sack covered the gauze for moisture storage.

Before the experiments were conducted, all specimens were placed in the experimental conditions for 1 week to ensure that

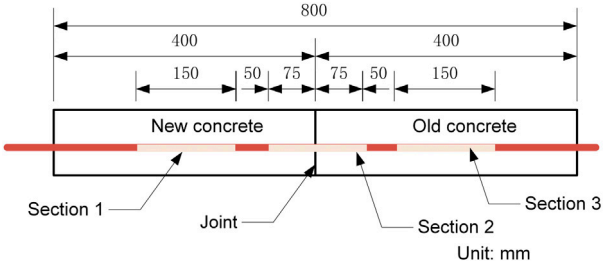

FIGURE 4
Sections of rebar.

the subsequent electrochemical reaction could formed an electrical circuit.

The initial current density was controlled at about 100 μA/cm^2, which was checked periodically to ensure its stability. In the dry stage of dry-wet cycles, the current density was significantly reduced. In order to reflect the influence of dry-wet cycle conditions, only the current density in the wet stage was stably controlled during the test. The corrosion time was set at 60 days.

After corrosion experiments, the specimens were broken, and the steel bars were taken out. The concrete adhering to the steel bars was scraped off. Then, the steel bars were pickled with 12% hydrochloric acid solution, rinsed, and dried for weighing.

After each full steel bar was accurately weighed, the mild steel bars and two types of stainless-steel bars were cut into multiple sections and three of them were taken. The length and position of the cut sections are shown in Figure 4. The length and weight of each section were accurately measured.

The weight loss rates of full rebars were calculated as follows:

$$L_\omega = \frac{\omega_0 - \omega}{\omega_0} \times 100\%$$

In the equation above L_ω is weight loss rate of the steel bar; ω_0 is the weight of the steel bar before corrosion (g); and ω is the mass of the corroded steel bar after pickling (g).

Assuming that the initial mass of steel bar was uniformly distributed along the length, the initial mass of each section was determined proportionally, and then the rust amount of each section was calculated. An influence coefficient of construction joint on local weight loss of a rebar was defined and calculated as follows:

$$k_j = \frac{2m_2}{m_1 + m_3}$$

In the equation above m_2 is the rust amount of the rebar in joint section 2 (g); m_1 is the rust amount of the rebar in non-joint section 1 (g); and m_3 is the rust amount of the rebar in non-joint section 3 (g).

3 Test results and discussion

3.1 Rust morphologies

Most of the specimens developed rust expansion cracks on the side of the concrete cover exposed to test conditions, as shown in Figure 5. All the cracks appeared along the direction of steel bars, and there were no cracks in the vertical direction of steel bars. No interface cracks developed at the joint, and the joint interface maintained good continuity before and after the test. Because the width of rust expansion cracks is affected by many factors such as the shape of bar and the presence of stirrups (Okazaki et al., 2020), the width of cracks in the experiments was not measured. However, by observing the cracks of all specimens, it was found that the crack widths of WD specimens (Figure 5A) were relatively larger than those of IC specimens (Figure 5B). In addition, the type of steel bar had a significant impact on the widths of the rust expansion cracks. The widths of cracks on mild steel specimens were obviously the largest, while those on stainless steel specimens were relatively small, and there were almost no visible cracks on specimens with epoxy-coated rebars.

The rust morphologies of rebars at different positions are shown in Figure 6.

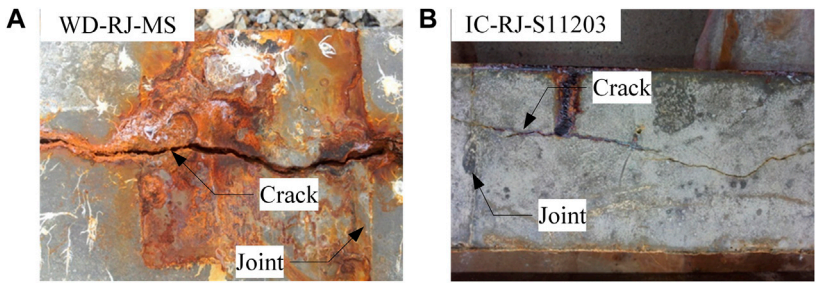

FIGURE 5
Rust expansion cracks on specimens. **(A)** WD-RJ-MS. **(B)** IC-RJ-S11203.

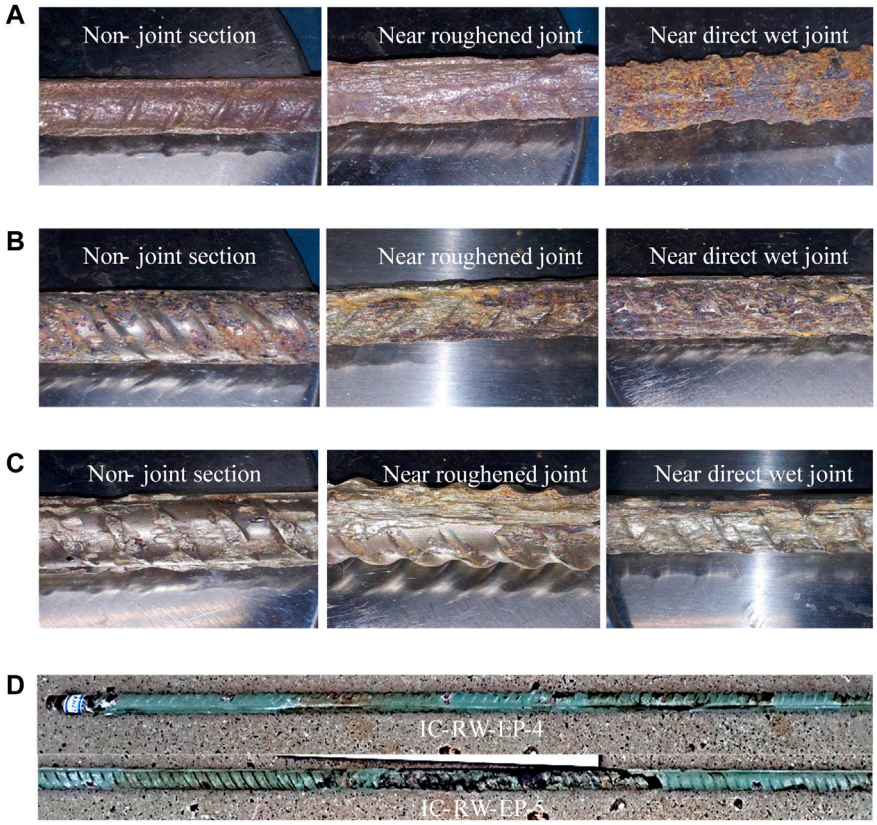

FIGURE 6
Rust morphologies of rebars. **(A)** Mild steel rebars. **(B)** S11203 rebars. **(C)** S23043 rebars. **(D)** Epoxy-coated steel rebars.

For mild steel bars (Figure 6A), the most severe corrosion of steel bars occurred at the joints. The corrosion developed from the joints to both sides. Most of mild steel bar surface was relatively smooth, some mild steel bars had longitudinal gullies, which was different from natural corrosion under pitting (Alonso et al., 2019). The corrosion of the non-joint section was more uniform along the surface of mild steel bar, and there was no obvious pitting corrosion. However, the concrete cover side of mild steel bar was more severely corroded than the backside, and the cross section of mild steel bar was elliptical after corrosion.

For S11203 stainless steel bars (Figure 6B), corrosion was mainly concentrated at the joints. The corrosion of the concrete cover side of S11203 bar was more severe, and no obvious corrosion was found on the side away from the cover. Moreover, the corrosion of S11203 bar at the joint was transversely fine and wavy, with less pit corrosion, which was quite different from that of mild steel bar. There were many corrosion pits and some corrosion spots on the surface of S11203 steel bar away from the joint.

The corrosion of S23043 stainless steel bar (Figure 6C) was similar to that of S11203. At the joints, the corrosion surface of S23043 bar was relatively smooth and the pitting corrosion was relatively less. However, far away from the joint, the corrosion pit of S23043 steel bar was larger and less intensive than that of S11203, which was probably because the composition of the two stainless steel bars was different. S23043 was a duplex stainless-steel bar, which was mainly composed of austenite and ferrite (Alonso et al., 2019), while S11203 was mainly composed of ferrite, and the chloride pitting resistance of ferrite was better than austenite (Chen 2020), so S23043 bar corrosion pit was generally larger.

The corrosion of epoxy-coated steel bars (Figure 6D) mainly occurred at the damage locations of epoxy coating (Sohail et al., 2019), not mainly at the joints. There were large corrosion pits at the damage locations, and brown rust adhered to the epoxy coating of the steel bars and the coating tended to peel off. When the epoxy coating at the joint was damaged and the damage was on the side of the concrete cover, the corrosion of the epoxy steel bar was the most severe, but there was no obvious corrosion on the backside.

Compared with mild steel bars, the rust of stainless-steel bars decreased from the joint to both sides more significantly and obviously. This phenomenon was due to the different

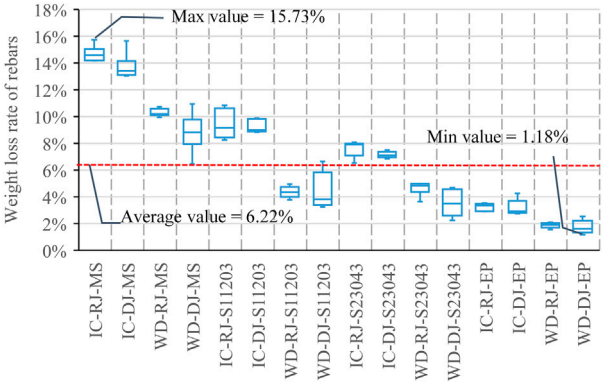

FIGURE 7
Weight loss rates of rebars.

content and form of iron in the two types of rebars. For mild steel bars with a high iron content, the electrolytic cells formed on the surface of rebars were more uniform, so the rust was more uniform. For stainless steel bars, because the iron was in the form of ferrite, austenite and other complexes, the large potential difference on the surface of rebars led to uneven distribution of the electrolytic cells. Therefore, the rust of the stainless-steel bars at the joints was relatively significant.

In general, except for epoxy-coated steel bars, the most severe corrosion of other steel bars all occurred at the joints, and the corrosion decreased from the joints to both sides, while the corrosion in non-joint sections was relatively uniform and less.

3.2 Weight loss rate of full bar

The box chart of the weight loss rate of all groups of full rebars is shown in Figure 7. There are no abnormal outliers in the figure. The average value of the weight loss rate of each group of specimens is shown in Table 4. The loss rate of specimens has the range of 1.18%–15.73% with an average value of 6.22%, which shows that there are big differences between different series.

3.3 Comparison of weight loss rate of full bar

In Figure 8, the box chart of the weight loss rate of rebars is shown by category. The figure shows that the average relationship of the weight loss rate of full rebars is mild steel bars > S11203 rebars > S23043 bars > epoxy-coated rebars. This means that the corrosion resistance of mild steel bars is the worst, and that of stainless-steel bars is better. Among them, the corrosion resistance of S23043 rebars is slightly better than that of S11203 rebars. The corrosion of

TABLE 4 Weight loss and percentage.

Id	$\overline{\omega_0}$ (g)	$\overline{\omega_0 - \omega}$ (g)	$\overline{L_\omega}$	$\overline{m_2}$ (g)	$\overline{0.5(m_1 + m_3)}$ (g)	$\overline{k_j}$
IC-RJ-MS	1222.77	179.53	14.68%	43.69	33.16	1.32
IC-DJ-MS	1219.92	167.34	13.71%	37.92	32.33	1.17
WD-RJ-MS	1215.06	125.11	10.29%	30.56	21.69	1.41
WD-DJ-MS	1212.00	106.77	8.81%	27.24	17.02	1.63
IC-RJ-S11203	1292.70	121.97	9.46%	36.28	20.97	1.73
IC-DJ-S11203	1308.09	121.36	9.28%	29.26	20.10	1.46
WD-RJ-S11203	1319.66	57.73	4.37%	19.14	9.74	1.97
WD-DJ-S11203	1302.69	58.20	4.46%	17.51	7.03	2.54
IC-RJ-S23043	1293.68	98.37	7.61%	28.51	18.19	1.57
IC-DJ-S23043	1258.18	89.91	7.14%	25.53	18.25	1.40
WD-RJ-S23043	1249.78	58.16	4.65%	18.42	7.99	2.33
WD-DJ-S23043	1251.76	44.12	3.53%	17.27	7.15	2.58
IC-RJ-EP	1288.80	41.61	3.23%	—	—	—
IC-DJ-EP	1288.36	41.11	3.19%	—	—	—
WD-RJ-EP	1286.85	24.19	1.88%	—	—	—
WD-DJ-EP	1283.91	22.39	1.74%	—	—	—

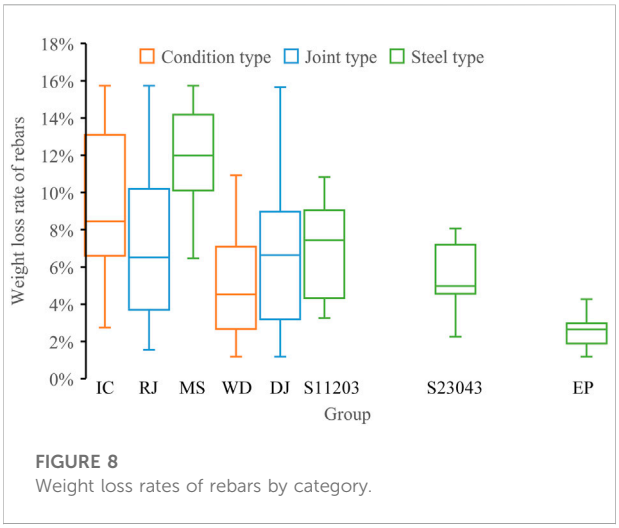

FIGURE 8
Weight loss rates of rebars by category.

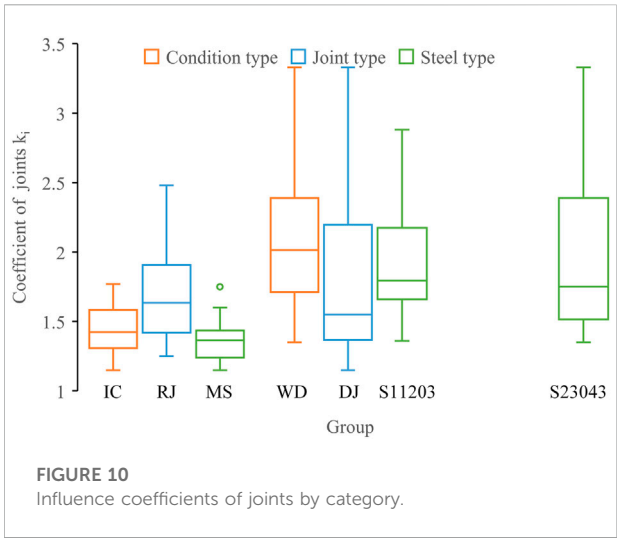

FIGURE 10
Influence coefficients of joints by category.

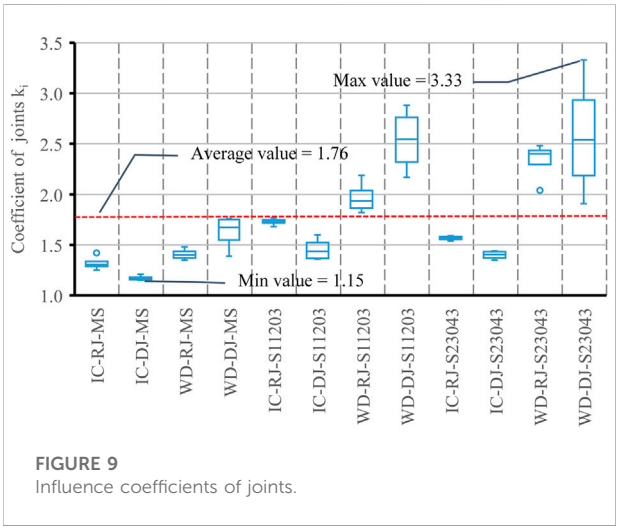

FIGURE 9
Influence coefficients of joints.

epoxy-coated rebars is the smallest, and the fluctuation is also the smallest.

From the perspective of joint type, the average rust amount of roughened wet joint (RJ) specimens is slightly greater than that of direct wet joint (DJ) specimens, and the fluctuations of the two categories are not much different. The ratio of the weight loss rate of RJ specimens to DJ specimens has an average value of 1.09. It is generally believed that the roughening is beneficial to the joint interface, which can make it better connect into a whole and conducive to load transfer (Santos and Julio 2011; Santos et al., 2012). However, experiments have shown that the interfacial scabbling deteriorates the compactness of the interface to a certain extent. The main reason may be that scabbling by a mechanism or high-pressure water flow causes certain damage to the concrete surface. This damage leads to micro-cracks on the surface of the concrete and makes it easier for chloride ions to pass through the concrete cover to the surface of the steel bars.

From the perspective of condition type, the rust amounts of rebars in the immersion environment are greater than that in the wet–dry cycle environment. The average ratio of weight loss rate is 1.71, but this does not mean that the immersion environment is more unfavorable than the wet–dry cycle environment. From the point of view of the test conditions, the energization time under the immersion environment was significantly longer, and the current in the dry environment stage under the wet–dry cycle environment was relatively small, which led to a slower electrochemical corrosion reaction.

3.4 Effect of joint on local weight loss

Considering that the corrosion resistance of epoxy steel bars was mainly determined by the quality of epoxy coating during the test time, the effect of concrete cover was less evident. Therefore, when the steel bars were cut off to compare the corrosion of joints and non-joints, the epoxy coated steel bars were excluded, and only the mild steel bars and two types of stainless steel bars were cut and weighed and analyzed.

The box diagram of the influence coefficient of construction joint on local weight loss (k_j) in 48 specimens is shown in Figure 9. The average rust amounts of rebars in the interception section and the average influence coefficient of construction joint on local weight loss are shown in Table 4. It can be seen that the rust amounts of steel sections at the joints of all concrete specimens are significantly greater than those of the non-joint sections. The influence coefficient of construction joint is in the range of 1.15–3.33, with an average value of 1.76. According to the experimental phenomena, the corrosion of each steel bar at the non-joint sections was relatively uniform, so the corrosion rate could be deduced by local weight loss in non-joint sections.

But the corrosion of steel bars at the joint sections are significantly higher than those of non-joint sections, the corrosion rate of steel bars may not effectively reflect this uneven phenomenon. So the influence coefficient of construction joint on local weight loss (k_j) can negatively reflected the influence of joints on the rust uniformity of rebars in concrete specimens with joints to some extent, and the construction joints are indeed a weakness of concrete durability.

In Figure 10, the box chart of the influence coefficient of construction joint on local weight loss is shown by category. The average influence coefficients of construction joint of mild steel bars, S11203 stainless steel bars, and S23043 stainless steel bars are 1.38, 1.92, and 1.97, respectively. The influence coefficients of construction joint of mild steel bars have relatively small fluctuation. The amount of rust in mild steel sections at construction joints is higher than that of stainless-steel sections as shown in Table 4, which is consistent with the aforementioned rust distribution of mild steel and stainless-steel bars. However, it can be concluded that the rust uniformity of mild steel bars affected by construction joints is relatively better, and the two types of stainless-steel bars have worse uniformity. Therefore, in coastal concrete structures using stainless steel reinforcement, it is recommended to consider the concentrated corrosion of steel bars that may occur at the joints.

The average influence coefficients of RJ specimens and DJ specimens are 1.72 and 1.80, respectively, and DJ specimens have more fluctuation as shown in Figure 10. From the perspective of the relationship of joint section and non-joint section, the interfacial roughening has no significant effect on the corrosion uniformity of rebars. However, the rust amounts of joint sections in RJ specimens are significantly greater than in DJ specimens as shown in Table 4. The ratio of the two ranges from 1.07 to 1.24, with an average value of 1.13, which is slightly larger than the ratio of the overall weight loss rate (1.09). This shows that roughening does cause certain defects to the faces on old concrete and affects the density of the joints. That is, roughening is to a certain extent unfavorable to the resistance to the penetration of chloride ions at construction joints.

The average influence coefficients of IC specimens and WD specimens are 1.44 and 2.07, respectively, and WD specimens have more fluctuation as shown in Figure 10. This indicates that the rust uniformity of rebars in the immersion environment is significantly lower than in the wet–dry cycle environment. The ratio of the two ranges from 0.54 to 0.97, with an average value of 0.72. This shows that the corrosion of rebars at the joints is more severe in the wet–dry cycle environment; that is, to say, the rust amounts of rebars in the immersion environment may be higher than in the wet–dry cycle conditions, but the wet–dry cycle conditions are relatively more unfavorable for the joints.

The test results showed that the construction joint had become the weakness of durability in concrete. According to the analysis of joint details and concrete characteristics, there were three main reasons. First, because of the difference of concrete pouring sequence, the construction joint is different from the general continuous casting concrete, and there is no coarse aggregate crossing distribution on the construction joint interface. Without the block of coarse aggregate, the transmission capacity of harmful substances in cement mortar is stronger. Secondly, in the early stage of hydration heat, the water in the newly casted concrete will migrate to the concrete substrate, resulting in an increase in the water-cement ratio of the fresh concrete near the interface, thereby reducing the durability of the interface. Finally, there are shrinkage differences in different casting ages of concrete. The restrained shrinkage will produce tensile strain in fresh concrete, which further deteriorates the durability of the interface.

4 Conclusion

In most of the reinforcement concrete structures, construction joint is common and even inevitable. This study deals with the effect of construction joint on corrosion of reinforcement in concrete. Based on experimental studies conducted, the following conclusions have been drawn:

1) Corrosion morphologies of four kinds of experimental steel bars in concrete were different. Except for epoxy-coated steel bars, the most severe corrosion of experimental steel bars all occurred at the joints, while the corrosion in non-joint sections was relatively uniform and less. The rust amounts of rebars at the joint sections were significantly greater than those of the non-joint sections, and the influence coefficient of construction joint on local weight loss is 1.15–3.33, with an average value of 1.76. And meanwhile, the corrosion of epoxy-coated steel bars mainly occurred at the damage locations of epoxy coating, not mainly at the joints.
2) Under the same environmental conditions and joint types, the corrosion resistance of stainless-steel bars and epoxy-coated steel bars at the joint is significantly better than that of mild steel bars. The corrosion uniformity of mild steel bars affected by joints is better, and that of stainless-steel bars is poor. Therefore, it is still necessary to pay attention to the concentrated corrosion of stainless-steel bars that may occur at joints in coastal concrete structures. The corrosion resistance of epoxy coated steel bars at the joint depended on the coating state.
3) The influence coefficients of construction joint on local weight loss in the immersion environment are significantly lower than that of the wet–dry cycle environment. This

indicated that the corrosion of rebars at the joints under the wet–dry cycle environment is more severe, and it is relatively unfavorable to the durability of the joints.

4) The interfacial roughening had no significant effect on the corrosion uniformity of rebars. However, roughening caused certain defects to the concrete at the joints, which was unfavorable for the resistance of the joints to the penetration of chloride ions.

Data availability statement

The original contributions presented in the study are included in the article/Supplementary Material, further inquiries can be directed to the corresponding author.

Author contributions

GH, BW, YS, and GL contributed to the design of this research and analyzed and discussed the results of this research. YS and GL contributed to the methodology and performance of the experiments, including specimen fabrication, the electrochemical acceleration corrosion testing, and preparing the initial draft. BW and LW reviewed, edited, and prepared the final draft of this manuscript.

Funding

This research was funded by National Key Research and Development Program of China (Grant number 2013CB036303) and Scientific Research Project of Powerchina Roadbridge Group Co., Ltd. (Grant number HHZ-JGY-FW-07).

Acknowledgments

The authors are also highly grateful to Jinxin LI for his important support in material preparation and measurements during the testing phase of this research.

Conflict of interest

Authors GH, BW, and LW were employed by the company Powerchina Roadbridge Group Co., LTD.

The authors declare that this study received funding from Scientific Research Project of Powerchina Roadbridge Group Co., Ltd. The funder had the following involvement in the study: study design, decision to publish, and preparation of the manuscript.

The remaining authors declare that the research was conducted in the absence of any commercial or financial relationships that could be construed as a potential conflict of interest.

Publisher's note

Supplementary Material

The Supplementary Material for this article can be found online at: https://www.frontiersin.org/articles/10.3389/fmats.2022.1094696/full#supplementary-material

References

Alonso, M. C., Luna, F. J., and Criado, M. (2019). Corrosion behavior of duplex stainless steel reinforcement in ternary binder concrete exposed to natural chloride penetration. *Constr. Build. Mater.* 199, 385–395. doi:10.1016/j.conbuildmat.2018.12.036

Andrade, C. (2019). Correction to: Propagation of reinforcement corrosion: Principles, testing and modelling. *Mat. Struct.* 53 (1), 1. doi:10.1617/s11527-019-1420-3

Chen, C. (2020). An electrochemical investigation of corrosion behavior of 316l austenitic stainless steel reinforcement in concrete exposed to acidic environment. *Int. J. Electrochem. Sci.* 15 (2), 1634–1642. doi:10.20964/2020.02.48

Choe, G., Shinohara, Y., Kim, G., Lee, S., Lee, E., and Nam, J. (2020). Concrete corrosion cracking and transverse bar strain behavior in a reinforced concrete column under simulated marine conditions. *Appl. Sci.* 10 (5), 1794. doi:10.3390/app10051794

Goyal, A., Pouya, H. S., Ganjian, E., and Claisse, P. (2018). A review of corrosion and protection of steel in concrete. *Arab. J. Sci. Eng.* 43 (10), 5035–5055. doi:10.1007/s13369-018-3303-2

Guoping, L., Fangjian, H., and Yongxian, W. (2011). Chloride ion penetration in stressed concrete. *J. Mat. Civ. Eng.* 23 (8), 1145–1153. doi:10.1061/(asce)mt.1943-5533.0000281

James, A., Bazarchi, E., Chiniforush, A. A., Aghdam, P. P., Hosseini, M. R., Akbarnezhad, A., et al. (2019). Rebar corrosion detection, protection, and rehabilitation of reinforced concrete structures in coastal environments: A review. *Constr. Build. Mater.* 224, 1026–1039. doi:10.1016/j.conbuildmat.2019.07.250

Júlio, E. N. B. S., Branco, F. A. B., and Silva, V. t. D. (2004). Concrete-to-concrete bond strength. Influence of the roughness of the substrate surface. *Constr. Build. Mater.* 18 (9), 675–681. doi:10.1016/j.conbuildmat.2004.04.023

Kara, I. B. (2021). Experimental investigation of the effect of cold joint on strength and durability of concrete. *Arab. J. Sci. Eng.* 46 (11), 10397–10408. doi:10.1007/s13369-021-05400-5

Koh, T. H., Kim, M. K., Yang, K. H., Yoon, Y. S., and Kwon, S. J. (2019). Service life evaluation of rc t-girder under carbonation considering cold joint and loading effects. *Constr. Build. Mater.* 226, 106–116. doi:10.1016/j.conbuildmat.2019.07.106

Li, G. P., Hu, H., and Ren, C. (2017). Resistance of segmental joints to carbonation. *ACI Mat. J.* 114 (1), 137–148. doi:10.14359/51689487

Li, G. P., Hu, H., and Ren, C. (2016). Resistance of segmental joints to chloride ions. *ACI Mat. J.* 113 (4), 471–481. doi:10.14359/51688931

Lollini, F., Carsana, M., Gastaldi, M., and Redaelli, E. (2019). Corrosion behaviour of stainless steel reinforcement in concrete. *Corros. Rev.* 37 (1), 3–19. doi:10.1515/corrrev-2017-0088

Mun, J.-M., and Kwon, S.-J. (2016). Evaluation of chloride diffusion coefficients in cold joint concrete considering tensile and compressive regions. *J. Korea Concr. Inst.* 28 (4), 481–488. doi:10.4334/jkci.2016.28.4.481

Okazaki, S., Okuma, C., Kurumatani, M., Yoshida, H., and Matsushima, M. (2020). Predicting the width of corrosion-induced cracks in reinforced concrete using a damage model based on fracture mechanics. *Appl. Sci.* 10 (15), 5272. doi:10.3390/app10155272

Ou, Y. C., and Nguyen, N. D. (2016). Influences of location of reinforcement corrosion on seismic performance of corroded reinforced concrete beams. *Eng. Struct.* 126, 210–223. doi:10.1016/j.engstruct.2016.07.048

Santos, D. S., Santos, P. M. D., and Dias-da-Costa, D. (2012). Effect of surface preparation and bonding agent on the concrete-to-concrete interface strength. *Constr. Build. Mater.* 37, 102–110. doi:10.1016/j.conbuildmat.2012.07.028

Santos, P. M. D., and Julio, E. N. B. S. (2011). Factors affecting bond between new and old concrete. *ACI Mat. J.* 108 (4), 449–456. doi:10.14359/51683118

Shen, Y., Liu, J., Zhou, S. Y., and Li, G. P. (2019). Experimental investigation on the freeze-thaw durability of concrete under compressive load and with joints. *Constr. Build. Mater.* 229, 116893. doi:10.1016/j.conbuildmat.2019.116893

Sohail, M. G., Salih, M., Al Nuaimi, N., and Kahraman, R. (2019). Corrosion performance of mild steel and epoxy coated rebar in concrete under simulated harsh environment. *Int. J. Build. Pathol. Adapt.* 37 (5), 657–678. doi:10.1108/Ijbpa-12-2018-0099

Song, H., Niu, D. T., and Li, S. H. (2008). "Comparison of electrochemical accelerated corrosion and corrosion in natural environment," in *Advances in concrete structural durability* (Hangzhou China: ICDCS 2008), 1130–1135.

Stern, M., and Geaby, A. L. (1957). Electrochemical polarization. *J. Electrochem. Soc.* 104 (1), 56. doi:10.1149/1.2428496

Sung-Won, Y., and Seung-Jun, K. (2016). Effects of cold joint and loading conditions on chloride diffusion in concrete containing ggbfs. *Constr. Build. Mater.* 115, 247–255. doi:10.1016/j.conbuildmat.2016.04.010

Vanlalruata, J., and Marthong, C. (2021). Effect of cold joint on the flexural strength of rc beam. *J. Struct. Integr. Maintenance* 6 (1), 28–36. doi:10.1080/24705314.2020.1823556

Yang, H.-M., Lee, H.-S., Yang, K.-H., Ismail, M. A., and Kwon, S.-J. (2018). Time and cold joint effect on chloride diffusion in concrete containing ggbfs under various loading conditions. *Constr. Build. Mater.* 167, 739–748. doi:10.1016/j.conbuildmat.2018.02.093

Yoon, Y.-S., Yang, K.-H., and Kwon, S.-J. (2020). Service life of ggbfs concrete under carbonation through probabilistic method considering cold joint and tensile stress. *J. Build. Eng.* 32, 101826. doi:10.1016/j.jobe.2020.101826

Yuan, W., Guo, A. X., Yuan, W. T., and Li, H. (2018). Shaking table tests of coastal bridge piers with different levels of corrosion damage caused by chloride penetration. *Constr. Build. Mater.* 173, 160–171. doi:10.1016/j.conbuildmat.2018.04.048

Zega, B. C., Prayuda, H., Monika, F., Saleh, F., and Wibowo, D. E. (2021). Effects of cold joint and its direction on the compressive and flexural strength of concrete. *Int. J. GEOMATE.* 20 (82), 86–92. doi:10.21660/2021.82.j2086

Zhou, H. J., Liang, X. B., Wang, Z. Q., Zhang, X. L., and Xing, F. (2017). Bond deterioration of corroded steel in two different concrete mixes. *Struct. Eng. Mech.* 63 (6), 725–734. doi:10.12989/sem.2017.63.6.725

Zhou, H. J., Lu, J. L., Xv, X., Zhou, Y. W., and Xing, F. (2015). Experimental study of bond-slip performance of corroded reinforced concrete under cyclic loading. *Adv. Mech. Eng.* 7 (3), 168781401557378. doi:10.1177/1687814015573787

Zhou, H. J., Xu, Y. N., Peng, Y. R., Liang, X. B., Li, D. W., and Xing, F. (2020). Partially corroded reinforced concrete piers under axial compression and cyclic loading: An experimental study. *Eng. Struct.* 203, 109880. doi:10.1016/j.engstruct.2019.109880